Rheologica Acta (2023) 62:15–30
https://doi.org/10.1007/s00397-022-01376-7

ORIGINAL CONTRIBUTION

Experimental separation of the onset of slip and sharkskin melt instabilities during the extrusion of silica-filled, styrene–butadiene rubber compounds

Alex Gansen[1] · Martin Řehoř[2] · Clemens Sill[3] · Patrycja Polińska[3] · Stephan Westermann[3,4] · Jean Dheur[3] · Jack S. Hale[2] · Jörg Baller[1]

Received: 29 October 2021 / Revised: 25 October 2022 / Accepted: 26 October 2022 / Published online: 23 November 2022

Abstract
The flow curves of polymers often reveal the onset of melt instabilities such as sharkskin, stick–slip, or gross melt fracture, in order of increasing shear rates. The focus of this work lies in the application of the Göttfert sharkskin option to the investigation of flow curves of styrene-butadiene rubber (SBR) compounds. The sharkskin option consists of highly sensitive pressure transducers located inside a slit die of a capillary rheometer. This tool allows the detection of in-situ pressure fluctuation characteristics of different melt instabilities. It is shown that the change of slope of the transition region in the flow curves is only linked to slip. Dynamic Mechanical Analysis (DMA) measurements furthermore show that the shear rate at which the change of slope can be observed shows the same temperature dependency as the viscous and elastic properties of the compounds.

Keywords SBR · Melt instabilities · Slip · Sharkskin · Stick–slip

Introduction

Ninety percent of the yearly global plastic production totalling 350 million tons is based on the following plastics, by order of weight produced: polyethylene (PE), polypropylene (PP), polyvinylchloride (PVC), polystyrene (PS), polyurethane (PU), and polyethylenterephtalate (PET) (Theconversation 2021). Therefore, the flow properties and melt instabilities of these polymers are of great interest. Natural and synthetic rubbers form a significant part of the remaining 10% in a ratio of 46% to 54% (Myrubbercouncil 2021) (Naue 2013). The analysis and understanding of melt instabilities are therefore of great interest to companies that make heavy use of rubber-based compounds in their products, such as the tire industry.

During industrial extrusion processes, melt instabilities represent a critical factor limiting maximum throughput, because they alter the properties of the extrudate. These melt instabilities typically appear with increasing shear rates and can roughly be classified as sharkskin, stick–slip, and gross melt fracture.

Sharkskin is a surface instability, as the height of the instability itself is small compared to the height of the extrudate. It appears as a highly regular periodic pattern across the entire surface of the extrudate, with an amplitude of a few tens of microns.

The stick–slip instability is characterized by alternating smooth and rough regions of the extrudate. It is accompanied by substantial pressure fluctuations ranging, e.g., for polyethylene samples extruded at 500 s^{-1} at a temperature of 180 °C from 2 to 11 bars measured by a pressure transducer in the barrel of a capillary rheometer (Filipe et al. 2008).

The last instability is referred to as gross melt fracture. In this case, the instability can exceed the height of the

✉ Jörg Baller
joerg.baller@uni.lu

[1] Department of Physics and Materials Science, University of Luxembourg, 162a Avenue de la Faïencerie, 1511 Luxembourg, Luxembourg

[2] Institute of Computational Engineering, University of Luxembourg, 6 Avenue de La Fonte, 4362 Esch-Sur-Alzette, Luxembourg

[3] Goodyear Innovation Center Luxembourg, Avenue Gordon Smith, 7750 Colmar-Berg, Luxembourg

[4] Functional Polymers Unit, Luxembourg Institute of Science and Technology, 5 Rue Bommel Z.A.E. Robert Steichen, 4940 Hautcharage, Luxembourg

extrudate which leads to a distortion of the whole extrudate. This is clearly undesirable in the majority of manufacturing situations.

The occurrence of different instabilities is dependent on the molecular weight, polydispersity, branching, etc. (Filipe et al. 2008). Not all melt instabilities occur for a specific polymer. Some polymers might only show sharkskin, whereas others only show stick–slip. But typically, sharkskin occurs at lower shear rates than stick–slip.

For general review articles about melt instabilities, we refer the reader to Agassant et al. (2006) and Vergnes (2015). The focus of this work is on the occurrence of melt instabilities for SBR compounds, as they show different behavior during the extrusion process compared with the aforementioned plastics. Often, thermoplastics like linear polyethylene (Merten et al. 2002) or polyethylene with short-chain branching ((Palza et al. 2010a, b), (Naue 2013)) show a smooth extrudate at low shear rates (in this case below 50 s^{-1}). Unfilled SBR, on the other hand, shows instabilities even at very low shear rates. For example, below 5 s^{-1} a very pronounced sharkskin instability (Viloria et al. 2017) can be observed.

Vergnes and Mongruel ((Vergnes 2015), (Viloria et al. 2017), (Mongruel & Cartault 2006)) have extensively studied the extrusion of unfilled SBR as well as of SBR compounds. To characterize melt instabilities, flow curves (wall shear stress or pressure vs shear rate) are mostly obtained by measurements with capillary rheometers. The flow curves can often be divided into three main regions. For a linear polyethylene, a typical flow curve displaying the different melt instabilities is shown in Fig. 1

A regular region (branch I) at low shear rates, where the wall shear stress increases steadily with the shear rate. Next, a region where the slope significantly decreases with respect to branch I might be observable. For samples showing stick–slip, pressure fluctuations of about 10% can be observed. If no stick–slip occurs, a plateau region still forms but without pressure oscillations. After the plateau, it might happen that the wall shear stress increases again significantly with the shear rate. This region is then referred to as branch II. For plastics, the change in the slope of the flow curve is typically associated with the onset of sharkskin (Hill et al. 1990), (Wang 1999), (Denn 2001). According to Viloria (Viloria et al. 2017), for SBR and SBR compounds, slip is, however, identified as the main reason for the change of slope in the flow curves.

In this paper, we further investigate the relation between melt instabilities and slip and especially their correlation with the different regions of the flow curve for SBR and SBR compounds. We use the sharkskin

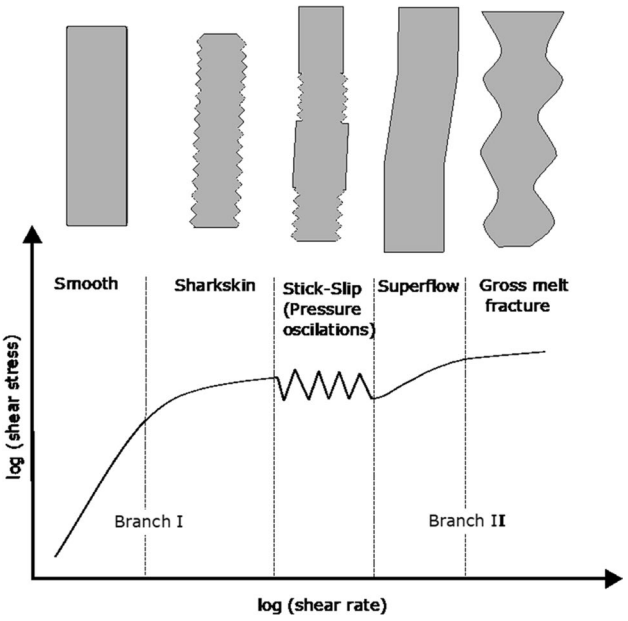

Fig. 1 Flow curve displaying different forms of extrusion instabilities for linear polyethylene

option developed by Wilhelm et al. (Filipe et al. 2008), (Naue et al. 2015), (Naue 2013) and commercialized by Göttfert GmbH to investigate if melt instabilities or slip are responsible for the change of slope in the flow curves

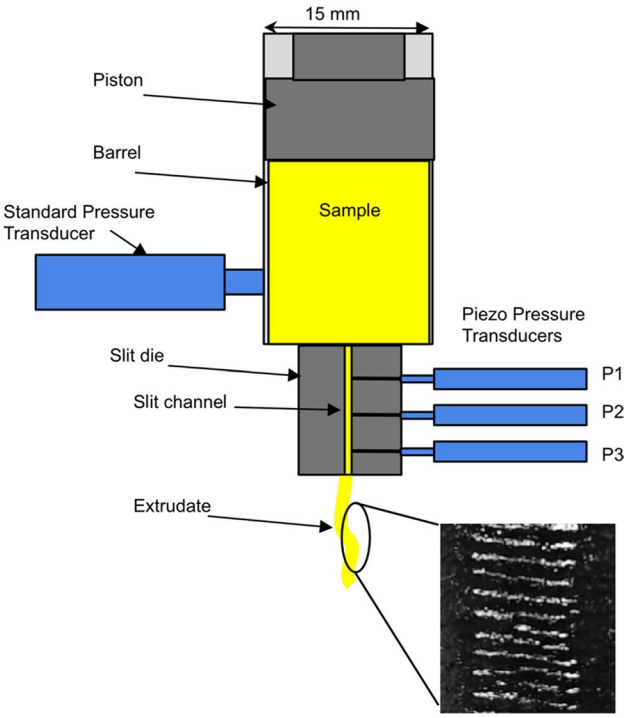

Fig. 2 Göttfert sharkskin option with three piezoelectric pressure transducers located alongside the die

of SBR compounds. It is furthermore investigated how fillers and temperature influence these instabilities and the onset of slip.

Materials and methods

Sample preparation and experimental methods

The samples under investigations are SBR polymers containing 27% of styrene and functionalized end chains designed to promote interaction with silica fillers. The molecular weight is medium with 310,000 g mol^{-1} (measured with GPC relative to standard polystyrene). The silica employed is Zeosil Premium 200 MP manufactured by Solvay SA. The employed compounds have silica contents of 0, 30, 70, and 112 phr (parts per hundred rubber).

The measurements with the sharkskin option were carried out with the capillary rheometer Reograph 50 from Göttfert GmbH with a slit die of a length of L = 30 mm, a width of W = 5 mm, and a height of H = 0.5 mm. For this slit die, three piezo transducers with a sampling rate of 20 kHz are located along the die. They are positioned at distances of 3, 15, and 27 mm from the die entry. A sketch of the capillary rheometer with the sharkskin option is shown in Fig. 2. It turned out that the absolute pressure data of sensor P1 did not deliver reasonable results. Therefore, only data from sensors P2 and P3 is discussed in this study.

For a selected shear rate, a constant pressure in the barrel needs to be reached first before a measurement with the sharkskin option is carried out. The operating time of the sharkskin option depends on the type of instability. As the sharkskin defect is typically characterized by a more or less periodic surface pattern with a frequency in the order

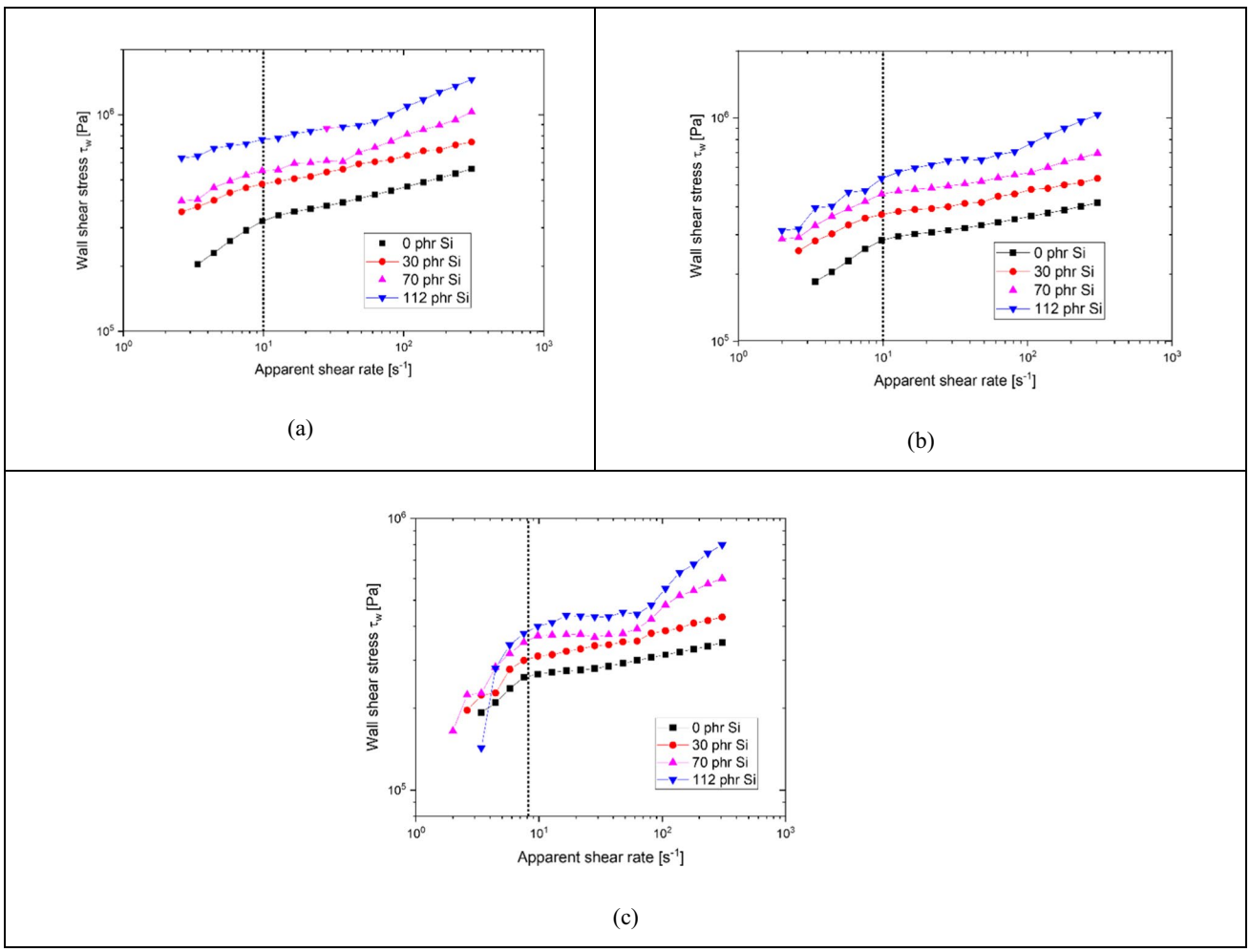

Fig. 3 Flow curves from a capillary rheometer for SBR compounds with 0 phr, 30 phr, 70 phr, and 112 phr silica at T = 80 °C and L/D ratios of **a** L/D = 5/1, **b** L/D = 10/1, and **c** L/D = 20/1

of 10 Hz, a relatively short operation time can be sufficient. The measurement time also depends on the shear rate. For lower shear rates, longer measurement times are required (up to 20 min). Using an optical analysis method described by Gansen et al. (2020), it was possible to confirm that 20 s is sufficient in our case.

For the stick–slip instability, which manifests itself through pressure oscillations of about 10% of the mean pressure, the characteristic frequency of the instability is far lower; in the order of 0.1 Hz. Therefore, measurement times of more than 120 s might be required. The time to extrude the sample is limited by the barrel size of the capillary rheometer as it may run out of material at high-volume flow rates. The piezoelectric pressure transducers then record the pressure oscillations over time. Applying the Fourier transform to the recorded pressure time series allows an identification of a specific instability with a corresponding frequency.

Flow curves

Before using the sharkskin option, which will be operated at specific shear rates, flow curves of the compounds are recorded to find the shear rates of interest.

The capillary rheometer Göttfert Rheograph 25 is used to obtain the flow curves of various SBR compounds for apparent shear rates from 2 s^{-1} to 300 s^{-1}. Measurements are carried out at 80 °C, 100 °C, and 120 °C using capillaries with different length-to-diameter ratios L/D = 5/1, 10/1, 20/1, and for unfilled SBR and SBR compounds with 30 phr, 70 phr, and 112 phr of silica.

As already discussed, the change of slope of the flow curve, or the possible onset and length of the plateau region depends on a variety of factors, including the molecular weight, filler content, shear rates, and temperature. The goal of the investigations is to understand

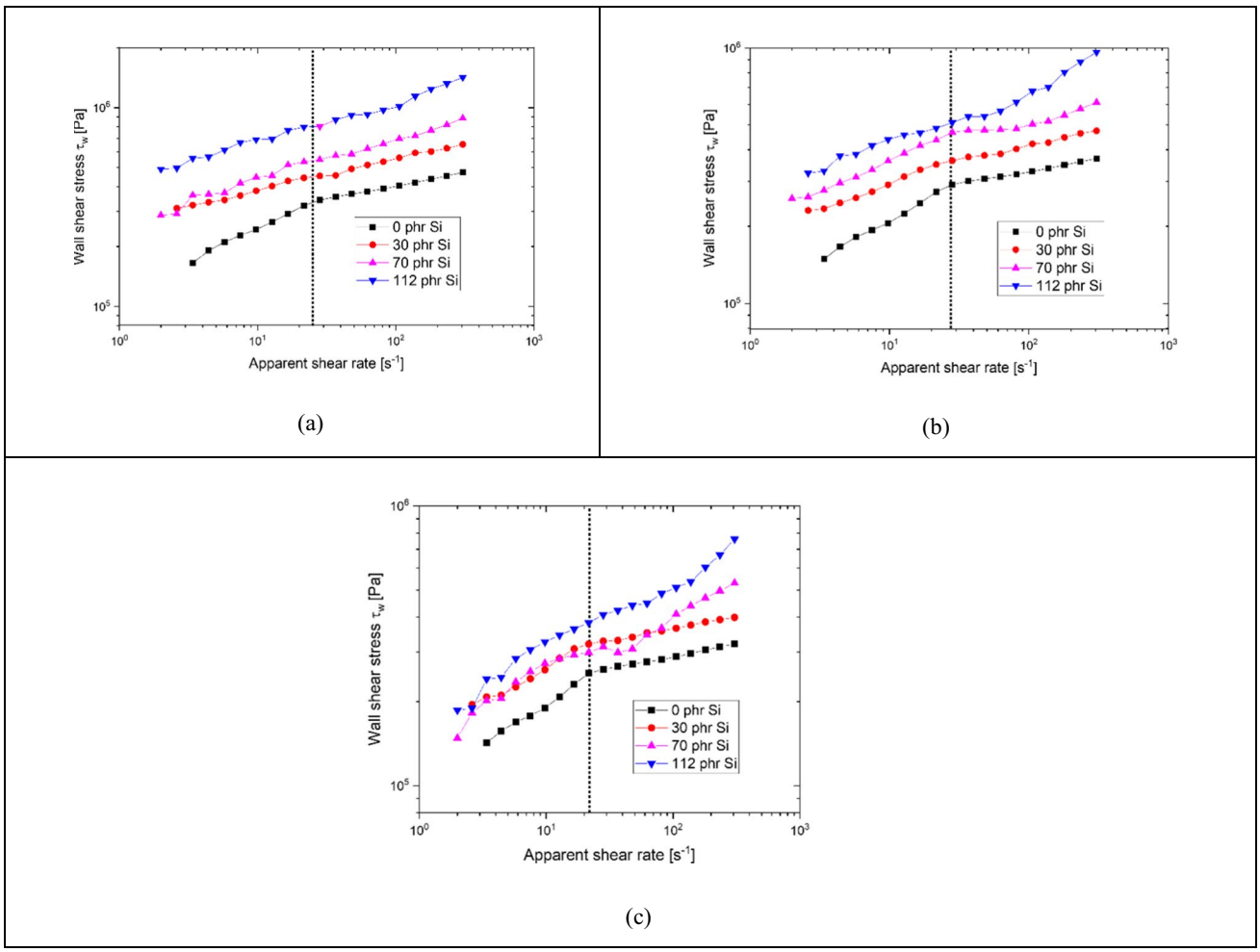

Fig. 4 Flow curves from a capillary rheometer for SBR compounds with 0 phr, 30 phr, 70 phr, and 112 phr silica at T = 100 °C and L/D ratios of **a** L/D = 5/1, **b** L/D = 10/1, and **c** L/D = 20/1

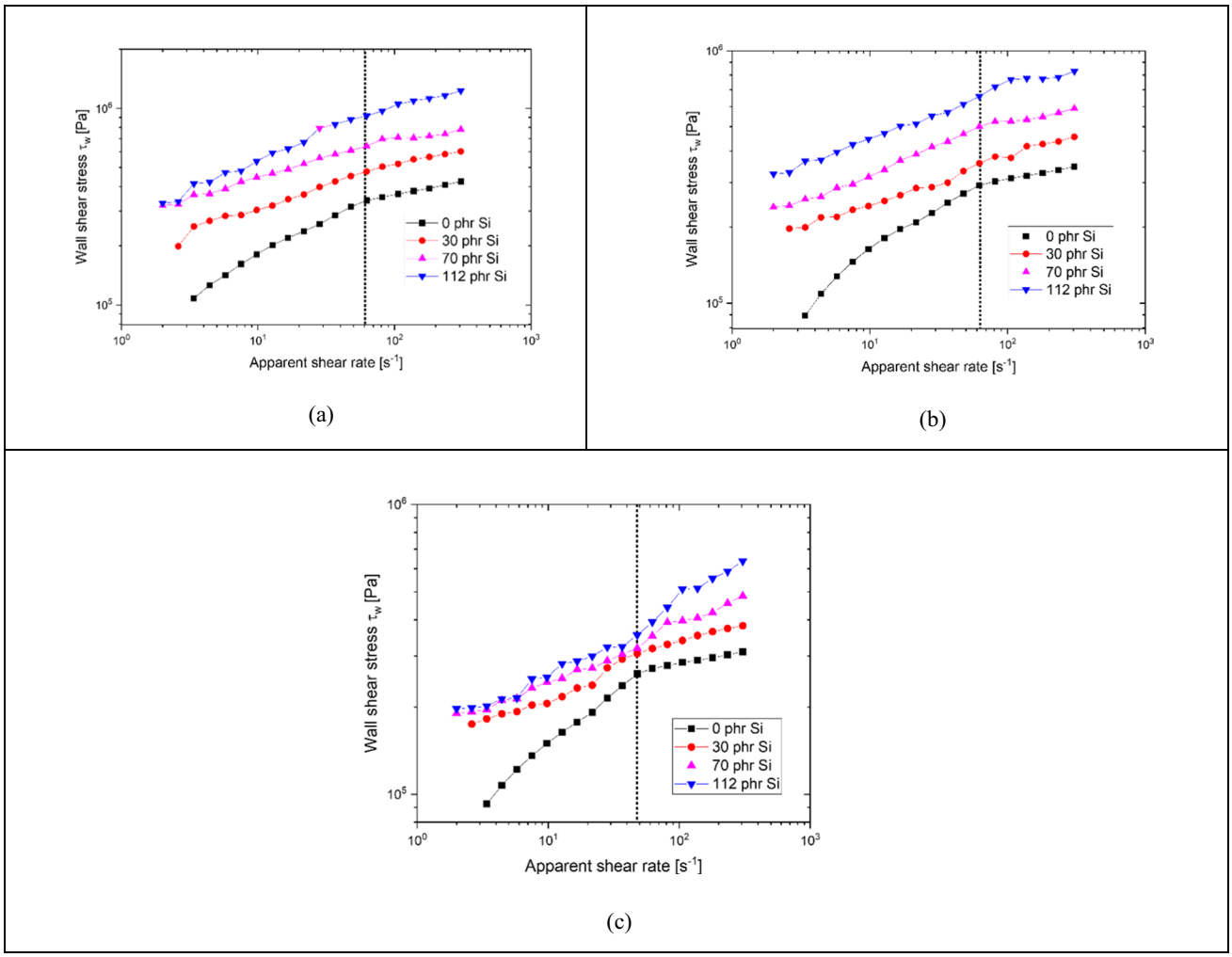

Fig. 5 Flow curves from a capillary rheometer for SBR compounds with 0 phr, 30 phr, 70 phr, and 112 phr silica at T = 120 °C and L/D ratios of **a** L/D = 5/1, **b** L/D = 10/1, and **c** L/D = 20/1

the dependency of the flow curves on the filler content, temperature, and die lengths. The aim is to find a configuration where a flow curve displays branch I, the change of slope, and branch II. From the flow curves, four shear rates are then selected for analysis. The first shear rate should be located in the branch I region, the second and the third at the beginning and end of the region with reduced slope, and finally, the last one, which should be located in the branch II region. To ensure reliable results, at least two sets of measurements are performed for each temperature, capillary, and compound.

Table 1 Shear rates $\dot{\gamma}_p$ associated with the change of slope of the flow curves (nearly independent of the silica content) and shift factors a_T used to construct the DMA master curves (Fig. 13) and the master curves of the flow curves (Fig. 14). For more information, see text

Temperature (°C)	$\dot{\gamma}_p$ (s^{-1})	log a_T from DMA master curves			log a_T from $\dot{\gamma}_p$
		0 phr	30 phr	70phr	
80	10	0.53	0.31	0.50	0.4
100	25	0	0	0	0
120	~80	−0.44	−0.24	−0.41	−0.5

Figures 3–5 show the flow curves for the compounds at three different temperatures. The dotted lines correspond to the change of slope of the unfilled SBR which acts as a reference. From Figs. 3–5, several conclusions can be drawn. Firstly, the change of slope (dotted lines) strongly depends on the temperature, as for increasing temperatures, the onset of slip is delayed to higher shear rates. Although the change of slope (dotted lines) is largely independent of the capillary length, a longer capillary leads to a more pronounced separation of branch I, the region with reduced slope, and

branch II as can be seen in Fig. 3a–c where the plateau region becomes more pronounced at T = 80 °C.

For T = 80 °C and the various capillary lengths (Fig. 3), the slope changes at a shear rate $\dot{\gamma}_{app} = 10\ s^{-1}$. For T = 100 °C (Fig. 4), the change of slope occurs at a shear rate $\dot{\gamma}_{app} = 25\ s^{-1}$ and for T = 120 °C at a shear rate of $\dot{\gamma}_{app} = 70\ s^{-1}$. It can be seen that only for T = 80 °C and especially for L/D = 10/1 and L/D = 20/1 (Fig. 3b–c), a plateau-like region with a reduced slope is formed. For the highly filled compounds, the slope changes at slightly higher shear rates compared to the unfilled system. This can be seen especially at T = 120 °C where for L/D = 10/1 (Fig. 5b); the unfilled SBR shows a slope change at $\dot{\gamma}_{app} = 70\ s^{-1}$, whereas for the 70 phr the slope starts to vary at $\dot{\gamma}_{app} = 80\ s^{-1}$ and for the 112 phr compound at $\dot{\gamma}_{app} = 90\ s^{-1}$.

Furthermore, as already confirmed by Vergnes (2015), a second branch, after the plateau, occurs only for filled systems with at least 50 phr of filler content. This becomes clear for the measurements carried out at T = 80 °C (Fig. 3) for the 70 phr and 112 phr samples. For these samples, it seems that the second branch becomes more pronounced with the increasing capillary length for a constant diameter (Fig. 3a vs Fig. 3c). As the slope change shifts to higher shear rates with increasing temperature, a second branch, after a plateau, is actually not or only barely displayed in the flow curves at T = 120 °C. Table 1 summarizes the shear rates associated with the change of slope in the flow curves.

To summarize, the change of slope is primarily dependent on temperature. Furthermore, the compounds under investigation do not show pressure oscillations in the plateau region, a characteristic of stick–slip (Palza et al. 2010a, b). This is a common finding for polymers with long-chain branching.

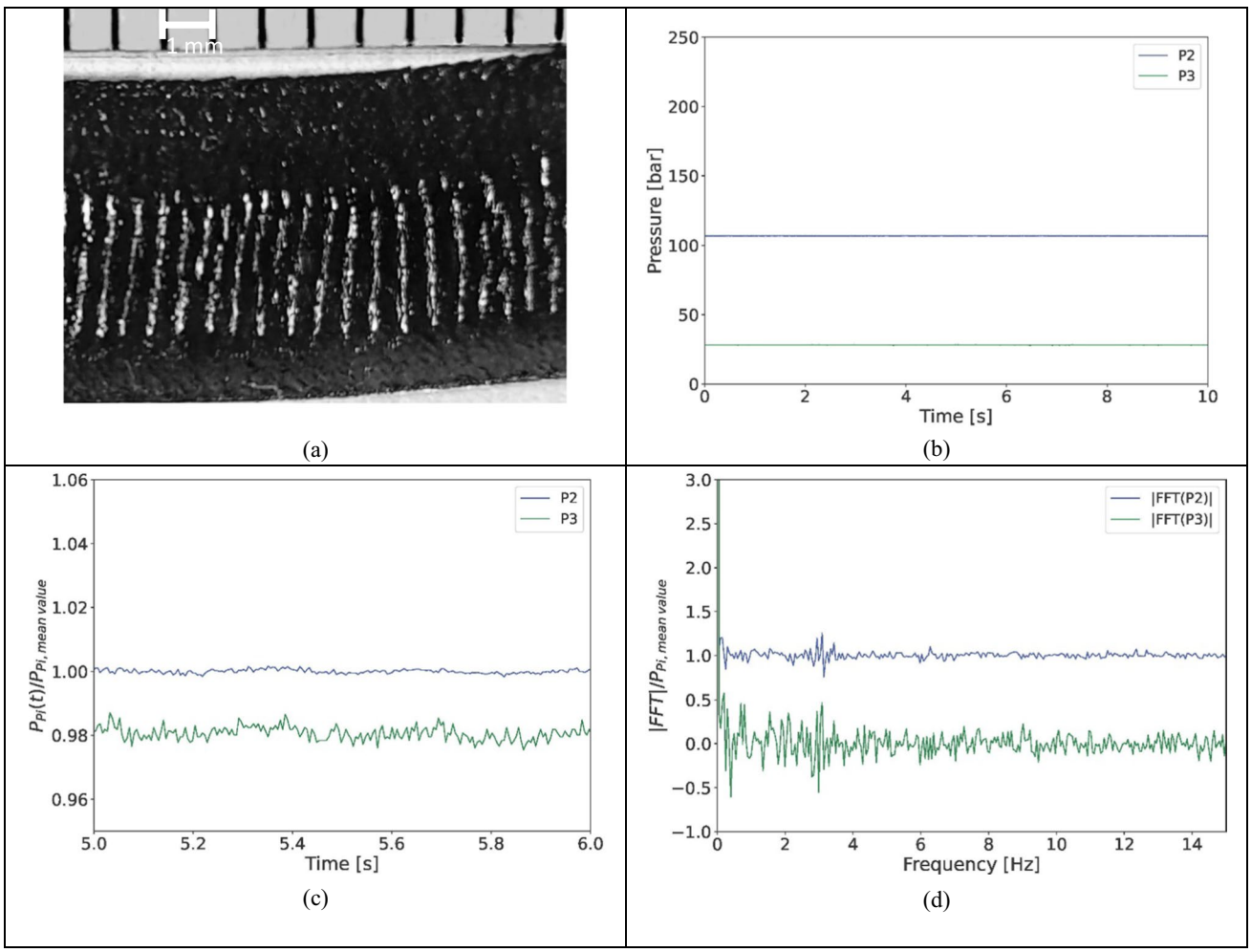

Fig. 6 Unfilled SBR extruded at a shear rate of $\dot{\gamma}_{app}$= 33 $s.^{-1}$.**a** Image (total length of 1 cm). **b** Pressure vs time over 10 s. **c** Zoom in for relative pressure vs time over 1 s (normalized and shifted vertically). **d** Relative FFT spectrum (normalized and shifted vertically)

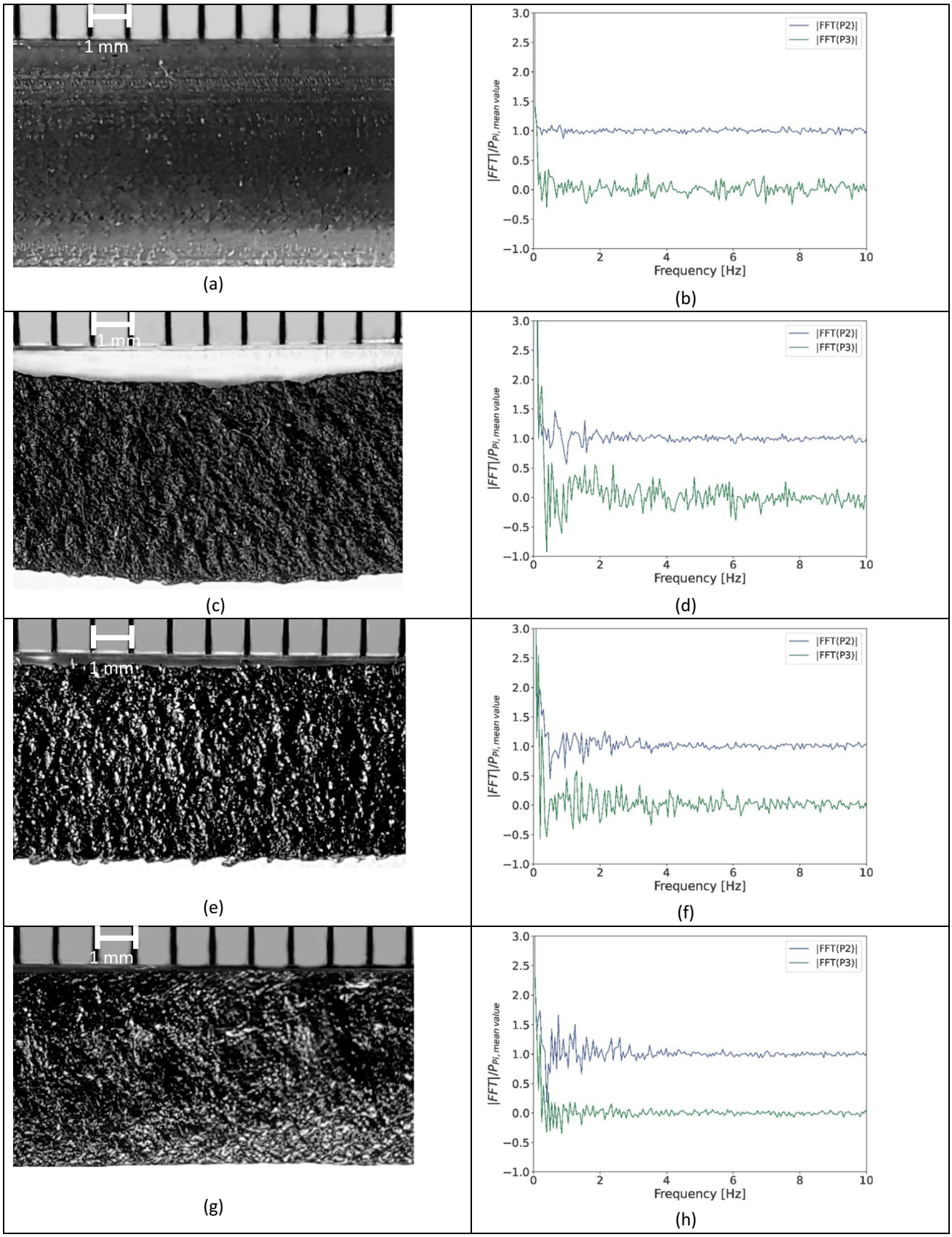

Fig. 7 Images of SBR and compounds filled with silica and corresponding FFT spectra extruded at $\dot{\gamma}_{app}$= 10 s^{-1}. **a**, **b** SBR + 0 phr Si **c**. **d** SBR + 30 phr Si. **e**, **f** SBR + 70 phr Si. **g**, **h** SBR + 112 phr Si

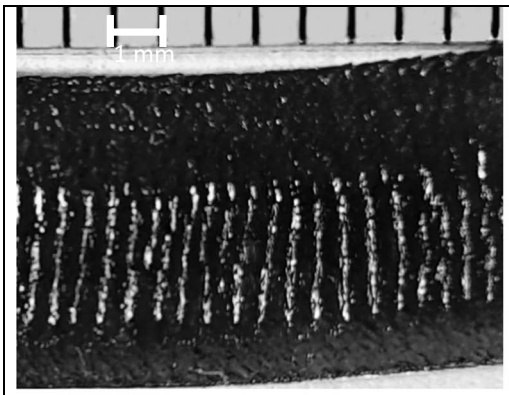
1 mm

(a)

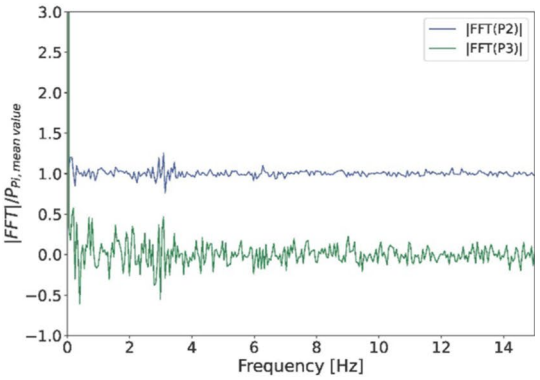
|FFT(P2)|
|FFT(P3)|
$|FFT|/P_{Pi,\,mean\,value}$
Frequency [Hz]

(b)

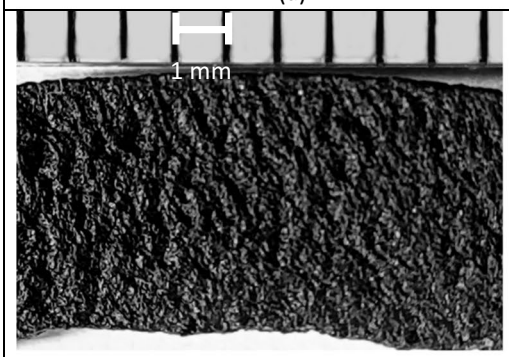
1 mm

(c)

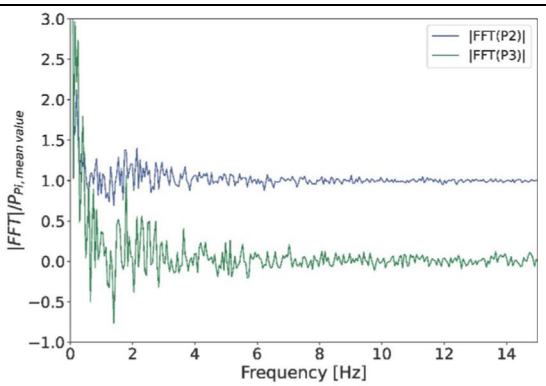
|FFT(P2)|
|FFT(P3)|
$|FFT|/P_{Pi,\,mean\,value}$
Frequency [Hz]

(d)

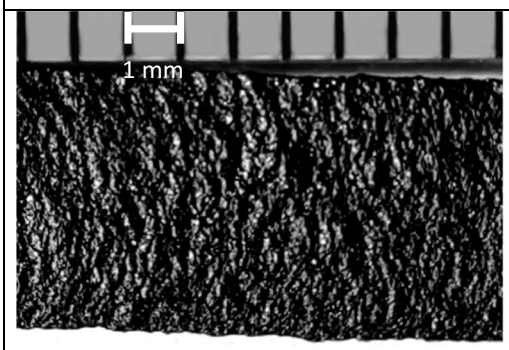
1 mm

(e)

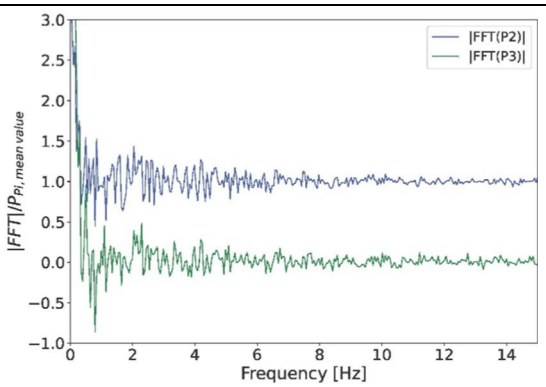
|FFT(P2)|
|FFT(P3)|
$|FFT|/P_{Pi,\,mean\,value}$
Frequency [Hz]

(f)

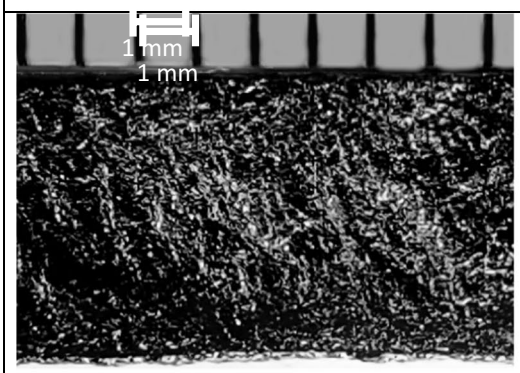
1 mm
1 mm

(g)

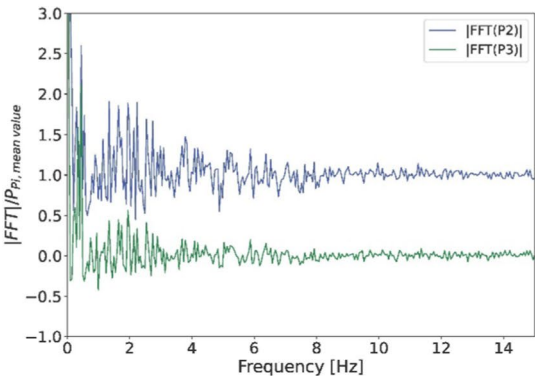
|FFT(P2)|
|FFT(P3)|
$|FFT|/P_{Pi,\,mean\,value}$
Frequency [Hz]

(h)

◂**Fig. 8** Images of SBR and compounds filled with silica and corresponding FFT spectra extruded at $\dot{\gamma}_{app}$= 33 s^{-1}.**a**, **b** SBR + 0 phr Si. **c**, **d** SBR + 30 phr Si. **e**, **f** SBR + 70 phr Si. **g**, **h** SBR + 112 phr Si

Results and discussion

Sharkskin option results

The sharkskin option employed for the presented measurements contains three piezoelectrical pressure transducers located along the slit die (Fig. 2). Only the signals from two of the three sensors (P2, P3) will be analyzed in the following (please cf. to section "Materials and Methods").

For each pressure transducer, a Fourier transform is applied to the pressure vs time signal. To illustrate this in the ideal case, unfilled SBR is extruded at T = 100 °C showing the sharkskin instability (Fig. 6a). The corresponding pressure signal for the two pressure transducers located inside the die is represented in Fig. 6b. The measurement time with the sharkskin option is fixed at 20 s. To better visualize the pressure oscillations over time, sometimes only a small fraction of the actual measurement is actually displayed. P2 is located in the middle of the die, followed by P3 close to the die exit. The two pressure signals seem to be largely constant over time. Normalizing each pressure signal by the mean pressure of the corresponding transducer, shifting them slightly vertically with respect to each other, and only representing a single second of the measurement leads to Fig. 6c. The two transducers clearly show periodic pressure fluctuations, approximately 3 s^{-1}. Therefore, a characteristic peak around 3 Hz is expected after applying the Fourier transform to the pressure signal. This is confirmed in Fig. 6d, where a characteristic peak appears at the same frequency for each pressure transducer after applying and normalizing the FFT (fast Fourier transformation). Using the optical analysis method (Gansen et al. 2020), we could confirm the result from the sharkskin option.

In Figs. 7–10, for each of the shear rates (10 s^{-1}, 33 s^{-1}, 60 s^{-1}, 200 s^{-1}), the FFT results from the sharkskin option of the SBR compounds are presented including a picture of the extrudate. The displayed extrudates all have a length of 1 cm. We do not show the pressure data for reasons of brevity. The results of the unfilled SBR clearly display an instability and act as a reference for the SBR compounds. For the evaluation of the characteristic frequency, the most pronounced peak (if there is more than one) has been considered. Each measurement with the sharkskin option was carried out at least twice to ensure reliable results. In a recent paper of Georgantopolus et al. (2021). the authors showed that the die geometry has an impact on the melt instability.

In a round hole capillary with L/D = 15 and D = 2 mm, their SBR showed the stick–slip instability at the shear rate range of 30 $s^{-1} \leq \dot{\gamma}_{app} \leq$ 60 s^{-1} whereas for a slit die with a length of L = 30 mm, a width of W = 5 mm, and a height of H = 0.5 mm; the instability is observed at 40 $s^{-1} \leq \dot{\gamma}_{app} \leq$ 300 s^{-1}. This means that the different shear rates linked to the different regions that have been selected from the flow curves might be slightly different for the shark skin option with the rectangular die. However, as pure SBR acts as the reference material the impact of the shear rate and silica content can clearly be seen by comparing them and it still matches the expectations from the flow curve.

For low shear rates, no instability was expected (branch I) whereas, for the plateau region and branch II, an instability was expected for pure SBR. Furthermore, the onset of the instability, typically associated with the plateau region is barely affected by changing the die geometry from the round hole to rectangular.

A shear rate of $\dot{\gamma}_{app}$ = 10 s^{-1} corresponds to branch I for T = 100 °C (Fig. 4), but the unfilled SBR shows already the emergence of first ripples at the surface (Fig. 7a) although they are not yet pronounced enough to be measured by the sharkskin option as no characteristic peak appears in Fig. 7b. The surface of the other compounds is significantly rougher but does not show a periodic pattern. Therefore, the FFT of the pressure signal shows some oscillations around 1 − 2 Hz for the 30 and 70-phr compound. This signal is measured for the 30 phr compound in each of the two pressure transducers. The resulting signal is not as narrow and strong as in Fig. 6d for the unfilled SBR. Maybe the shreds appearing at the bottom and top sides of the extrudate (Fig. 7e) lead to this as there are about 10 shreds on a length of 1 cm. The shear rate of $\dot{\gamma}_{app}$ = 10 s^{-1} corresponds for the used slit die to an extrusion speed of 0.83 mm/s. At this speed, it takes about t = 10/0.83 ≈ 12 s to produce 10 mm of the extrudate. Ten shreds in 12 s correspond to a frequency of about 0.83 Hz which is in a reasonable agreement with the FFT results. The 112 phr (Fig. 7g) compound shows a significantly different surface and no clear peak in the FFT (Fig. 7h) can be identified. Furthermore, no shreds are visible on the sides.

At a shear rate of $\dot{\gamma}_{app}$ = 33 s^{-1}, at the beginning of the plateau region for T = 100 °C (Fig. 4), a pronounced periodic pattern appears for the unfilled SBR (Fig. 8a) leading to a characteristic frequency of roughly 3 Hz which can be identified on the two pressure transducers. It should, however, be noted that the sharkskin also appeared at shear rates before the plateau region. Additional measurement that we did already showed the emergence of sharkskin at shear rates of $\dot{\gamma}_{app}$ < 5 s^{-1}, in agreement with observations from Viloria (Viloria

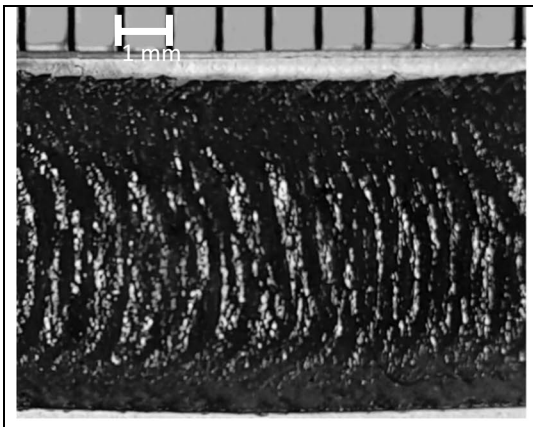
1 mm

(a)

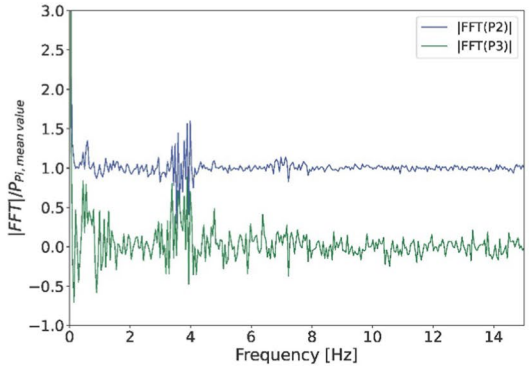
|FFT(P2)|
|FFT(P3)|
|FFT|/P_i, mean value
Frequency [Hz]

(b)

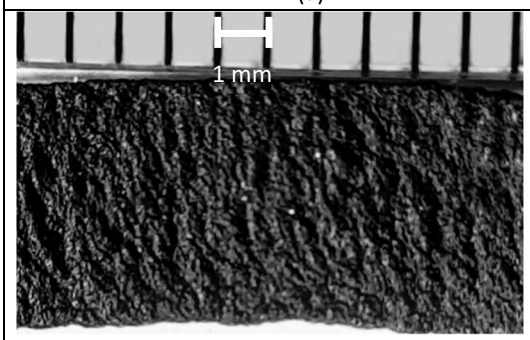
1 mm

(c)

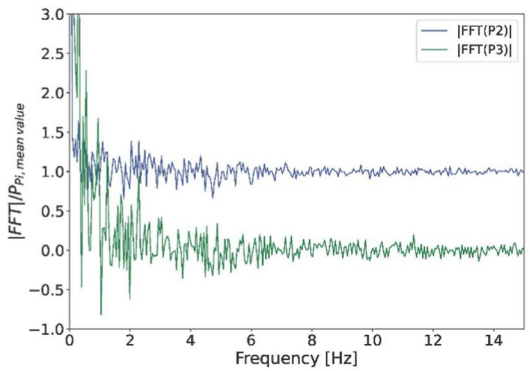
|FFT(P2)|
|FFT(P3)|
|FFT|/P_i, mean value
Frequency [Hz]

(d)

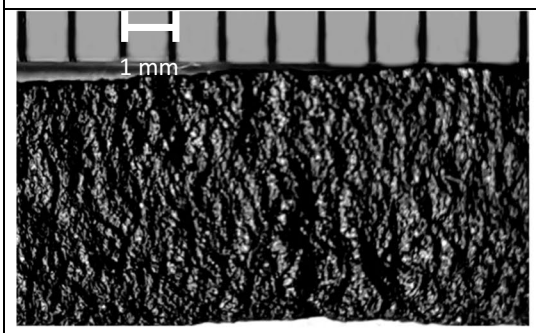
1 mm

(e)

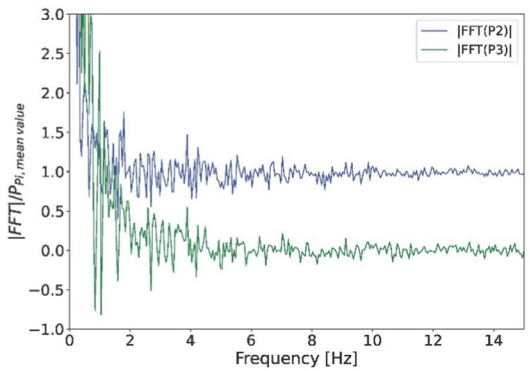
|FFT(P2)|
|FFT(P3)|
|FFT|/P_i, mean value
Frequency [Hz]

(f)

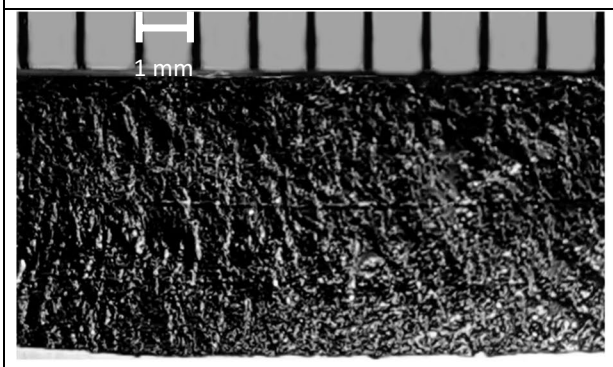
1 mm

(g)

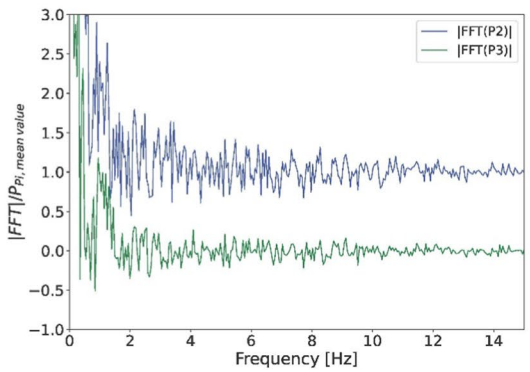
|FFT(P2)|
|FFT(P3)|
|FFT|/P_i, mean value
Frequency [Hz]

(h)

◂**Fig. 9** Images of SBR and compounds filled with silica and corresponding FFT spectra extruded at $\dot{\gamma}_{app} = 60\ s^{-1}$ **a**, **b** SBR + 0 phr Si. **c**, **d** SBR + 30 phr Si. **e**, **f** SBR + 70 phr Si. **g**, **h** SBR + 112 phr Si

et al. 2017). There does not appear to be a direct relation between the melt instability and the change of slope for the rubbers under investigation. This is contrary to the publication of Palza et al. (Palza et al. 2010a, b) which used the sharkskin option to investigate an ethylene/1-octene copolymer from Dow with a short-chain branching of 7 mol% referred to as PE-7 SCB in the corresponding paper. According to their results, "… PE-7 SCB developed the sharkskin instability as a surface distortion appears in the extrudate. Therefore, the slope change in the flow curve for this sample is due to the beginning of the sharkskin instability associated with the presence of short chain branching."

With the corresponding die dimension, $\dot{\gamma}_{app} = 33\ s^{-1}$ corresponds to 2.75 mm/s. At this speed, it takes about t = 10 mm/2.75 mm/s ≈ 3.6 s to produce 10 mm of the extrudate. Roughly, 20 shreds in 3.6 s correspond to a frequency of about 5.5 Hz which is in a reasonable agreement with the main FFT peak at 3 Hz. As explained in Palza et al. (2009), (Gansen et al. 2020) a similar difference between the characteristic frequencies from an optical comparison and pressure data is obtained. Palza et al. (Palza et al. 2009) investigated a polyethylene sample at an apparent shear rate of 315 s^{-1}. The characteristic frequency from the pressure data is 22 Hz whereas the characteristic frequency, deduced from an optical microscope picture of the extrudate, is 60 Hz. The order of magnitude of both characteristic frequencies is the same. The difference might occur due to the change from laminar to plug flow, errors in the extrudate velocity, or contraction of the extrudate.

A higher amplitude of the relative FFT for the sharkskin instability would be expected in the third pressure sensor closer to the die exit, as it is often referred to as the die exit effect. The origin of this peak is not entirely clear, as it does not appear in the other graphs (Fig. 8c–h). The following filled samples (30 phr, 70 phr, 112 phr of silica, Fig. 8d, f, and h) all show a peak or a higher amplitude between 1.5 Hz – 3 Hz. No instability can be identified in the corresponding pictures (Fig. 8c, e, and g). Furthermore, it seems that oscillations in the FFT shift to higher frequencies with increasing silica content. This is as expected, as for the unfilled SBR a clear periodic instability exists; therefore, a rather narrow response at a characteristic frequency of the FFT signal is expected. For the other filled samples, the material becomes stiffer due to the increasing silica content, and the surface becomes rougher without displaying any periodic pattern. Figure 8c, for example, shows a more pronounced irregular surface roughness compared to Fig. 8g, where more, but less pronounced features appear on the surface which results in an FFT signal broadened to higher frequencies (Fig. 8d vs Fig. 8h).

A shear rate of $\dot{\gamma}_{app} = 60\ s^{-1}$ corresponds to the end of plateau region for T = 100 °C (Fig. 4). For unfilled SBR (Fig. 9) at this shear rate, the sharkskin instability becomes even more pronounced (Fig. 9a) compared to the $\dot{\gamma}_{app} = 33\ s^{-1}$ displayed in Fig. 8a. The characteristic peak at $\dot{\gamma}_{app} = 60\ s^{-1}$ in the FFT spectrum slightly shifts to 3.5 Hz (Fig. 9b) compared to 3 Hz for $\dot{\gamma}_{app} = 33\ s^{-1}$ (Fig. 8b) and is also more pronounced. Similarly for the unfilled SBR extruded at $\dot{\gamma}_{app} = 33\ s^{-1}$ where a second, less pronounced peak appeared at 6 Hz, (Fig. 8b), a second peak appears at 7.5 Hz at a shear rate of $\dot{\gamma}_{app} = 60\ s^{-1}$ (Fig. 9b). For the filled compounds (Fig. 9c–h), the FFT spectrum does not reveal a major or minor characteristic peak but shows again a broader response in the FFT from 0 Hz up to 6 Hz similar to the $\dot{\gamma}_{app} = 33\ s^{-1}$ case.

A shear rate of $\dot{\gamma}_{app} = 200\ s^{-1}$ corresponds to branch II in the flow chart at T = 100 °C (Fig. 4). The unfilled SBR sample displays now a volume instability, a wavy pattern expanding from one to the other side of the extrudate (Fig. 9a). Two characteristic peaks appear in the corresponding FFT spectrum (Fig. 10b).

The first peak is located at 4 Hz for a shear rate $\dot{\gamma}_{app} = 200\ s^{-1}$. The characteristic frequency slightly increases as it was located before at 3 Hz and 3.5 Hz for the $\dot{\gamma}_{app} = 33\ s^{-1}$ and $\dot{\gamma}_{app} = 60\ s^{-1}$ shear rates. An additional peak appears at 14 Hz. A similar, less pronounced peak also occurs for the unfilled rubber at shear rates $\dot{\gamma}_{app} = 33\ s^{-1}$ and $\dot{\gamma}_{app} = 60\ s^{-1}$ respectively (Fig. 8b, 9b). This second frequency seems to have its origin inside the barrel as it is most pronounced in the FFT of the pressure transducer P1, closest to the die entry (Fig. 8b, 9b). Only at a shear rate of $\dot{\gamma}_{app} = 200\ s^{-1}$, the unfilled SBR shows a strong signal in the third pressure transducer P3, closest to the die exit (Fig. 10b). For all the other compounds (Fig. 10c, h), no characteristic peaks appear at all.

Local pressure inside the die

The FFT used in the previous sections is applied to the pressure data. Figure 11a and d contain the pressure data for the unfilled SBR and Fig. 12a–d the pressure data for the 70 phr compound. As mentioned before, the piezoelectrical pressure sensors P2 and P3 are located at 15 mm and 27 mm from the die entry respectively. Therefore, it is expected that the pressure is highest at P2 and lowest at P3. This is confirmed by Fig. 11a–d.

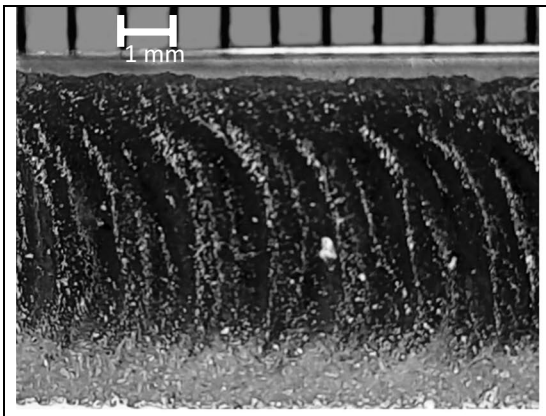
1 mm

(a)

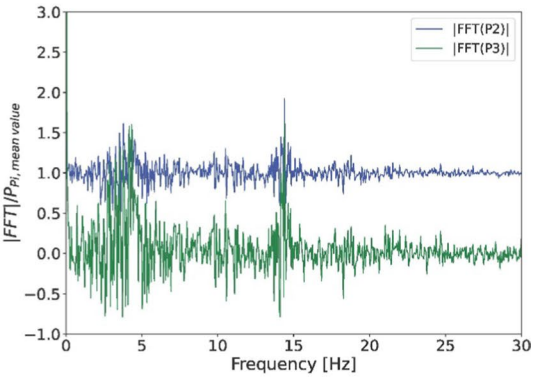
|FFT(P2)|
|FFT(P3)|
|FFT|/P_Pi, mean value
Frequency [Hz]

(b)

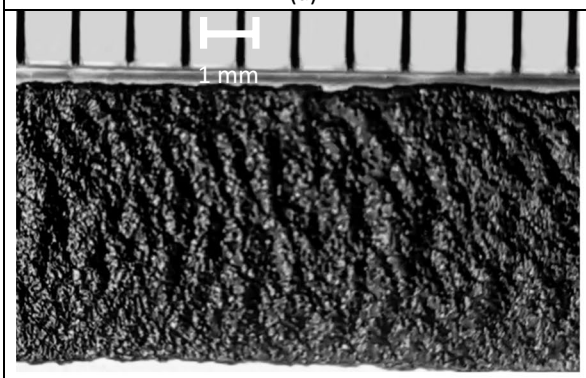
1 mm

(c)

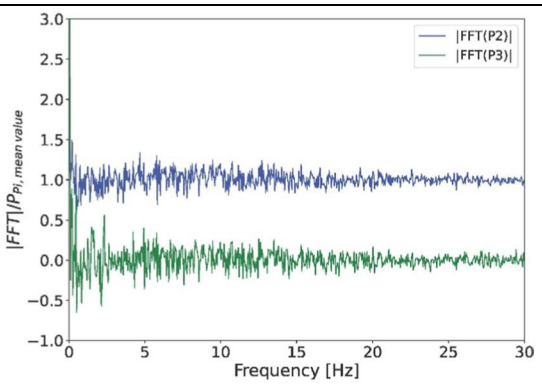
|FFT(P2)|
|FFT(P3)|
|FFT|/P_Pi, mean value
Frequency [Hz]

(d)

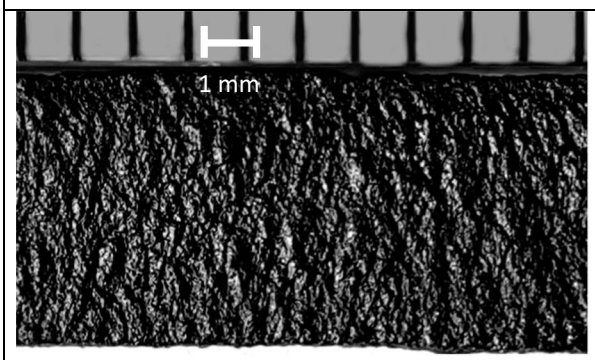
1 mm

(e)

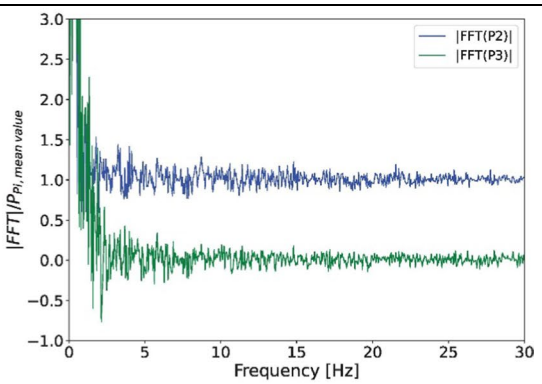
|FFT(P2)|
|FFT(P3)|
|FFT|/P_Pi, mean value
Frequency [Hz]

(f)

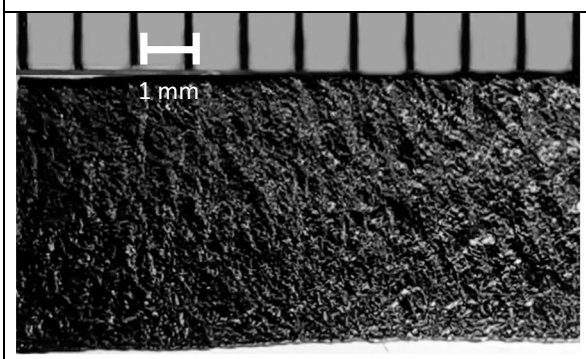
1 mm

(g)

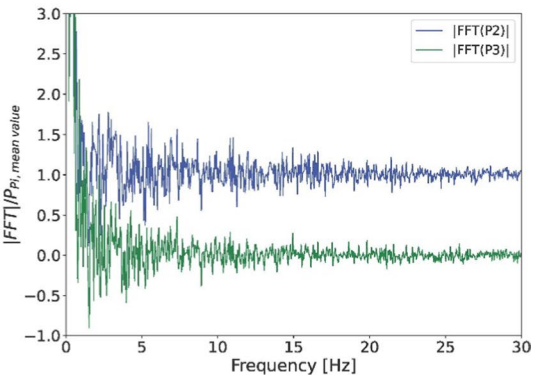
|FFT(P2)|
|FFT(P3)|
|FFT|/P_Pi, mean value
Frequency [Hz]

(h)

◂**Fig. 10** Images of SBR and compounds filled with silica and corresponding FFT spectra extruded at $\dot{\gamma}_{app} = 200\ s^{-1}$ **a**, **b** SBR + 0 phr Si. **c**, **d** SBR + 30 phr Si. **e**, **f** SBR + 70phr Si. **g**, **h** SBR + 112phr Si

Master curves

Figures 3, 4, and 5 show that the apparent shear rates $\dot{\gamma}_p$ at which the change of slope appears are independent of the silica loadings but shifts with temperature. Crié et al. (Crié et al. 2015) showed that a master curve can be constructed from the individual flow curves of carbon-filled SBR compounds. Mongruel and Cartault (Mongruel & Cartault 2006) determined a so-called concentration shift factor which allows the construction of a master curve representation for the elastic moduli of silica and carbon black-filled SBR compounds. The focus of this section is now to investigate if the shift of $\dot{\gamma}_p$ with temperature is related to the temperature dependency of the viscoelastic properties of the compounds or if the temperature shift is independent from it.

Therefore, the shear moduli G′ and G″ of the compounds have been determined as a function of frequency and temperature by recording isothermal frequency sweeps at 17 different temperatures with Dynamic Mechanical Analysis (DMA). For the 112 phr compound, the DMA measurements did not give reliable data, therefore the analysis of this compound has been omitted in the following discussion. To construct the master curves from the isothermal frequency sweeps, we have exploited the temperature-frequency equivalence principle which allows superposing the storage and loss shear moduli by horizontal shifts log a_T along the angular frequency axis:

$$\omega(T_0) = \omega(T) \cdot a_T$$

As reference temperature, $T_0 = 100$ °C was chosen. Vertical shifts of the data were neglectable. The left side of

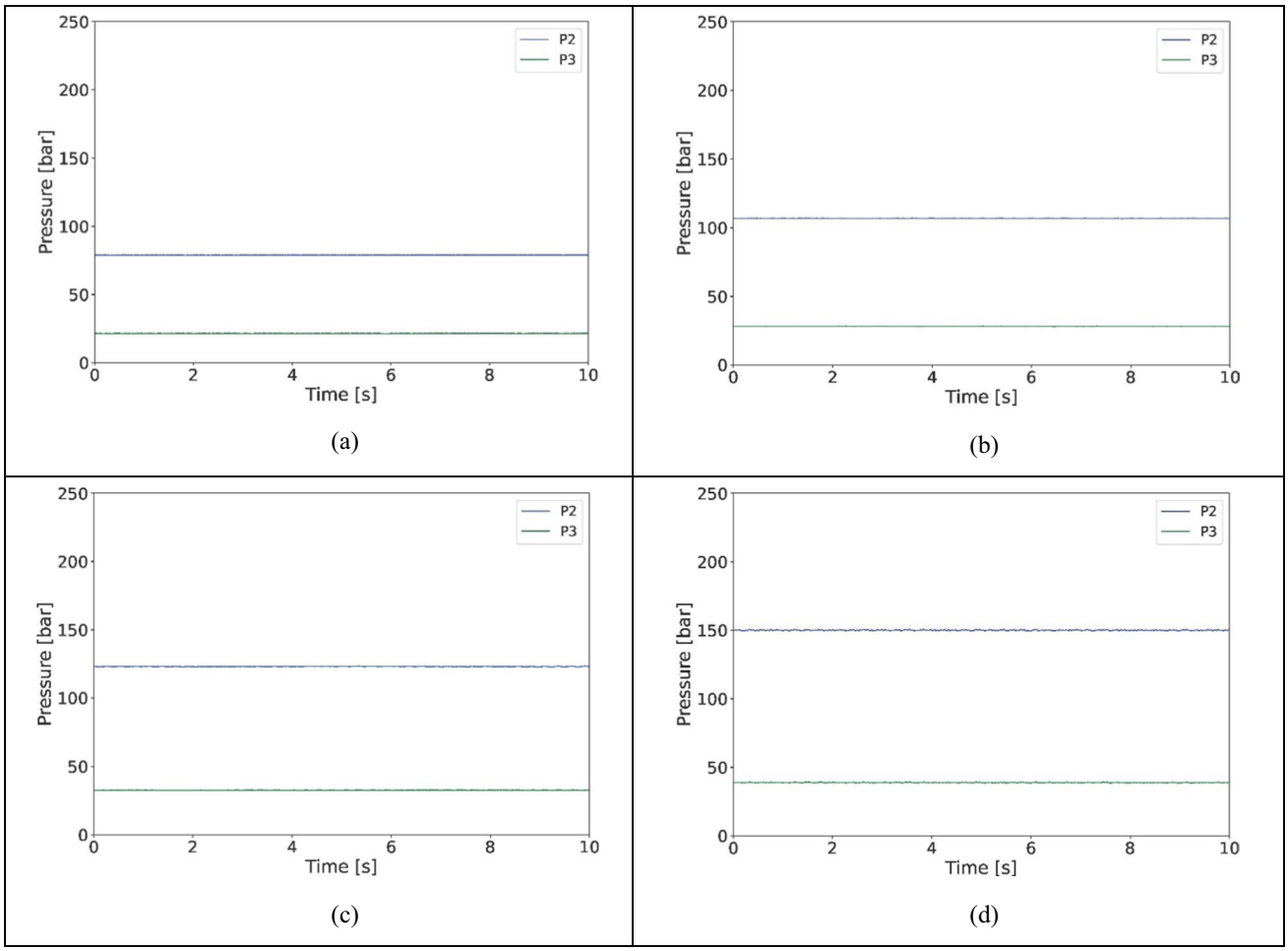

Fig. 11 Pressure data recorded with the sharkskin option for unfilled SBR at shear rates **a** $\dot{\gamma}_{app} = 10\ s^{-1}$, **b** $\dot{\gamma}_{app} = 33\ s^{-1}$, **c** $\dot{\gamma}_{app} = 60\ s^{-1}$, and **d** $\dot{\gamma}_{app} = 200\ s.^{-1}$

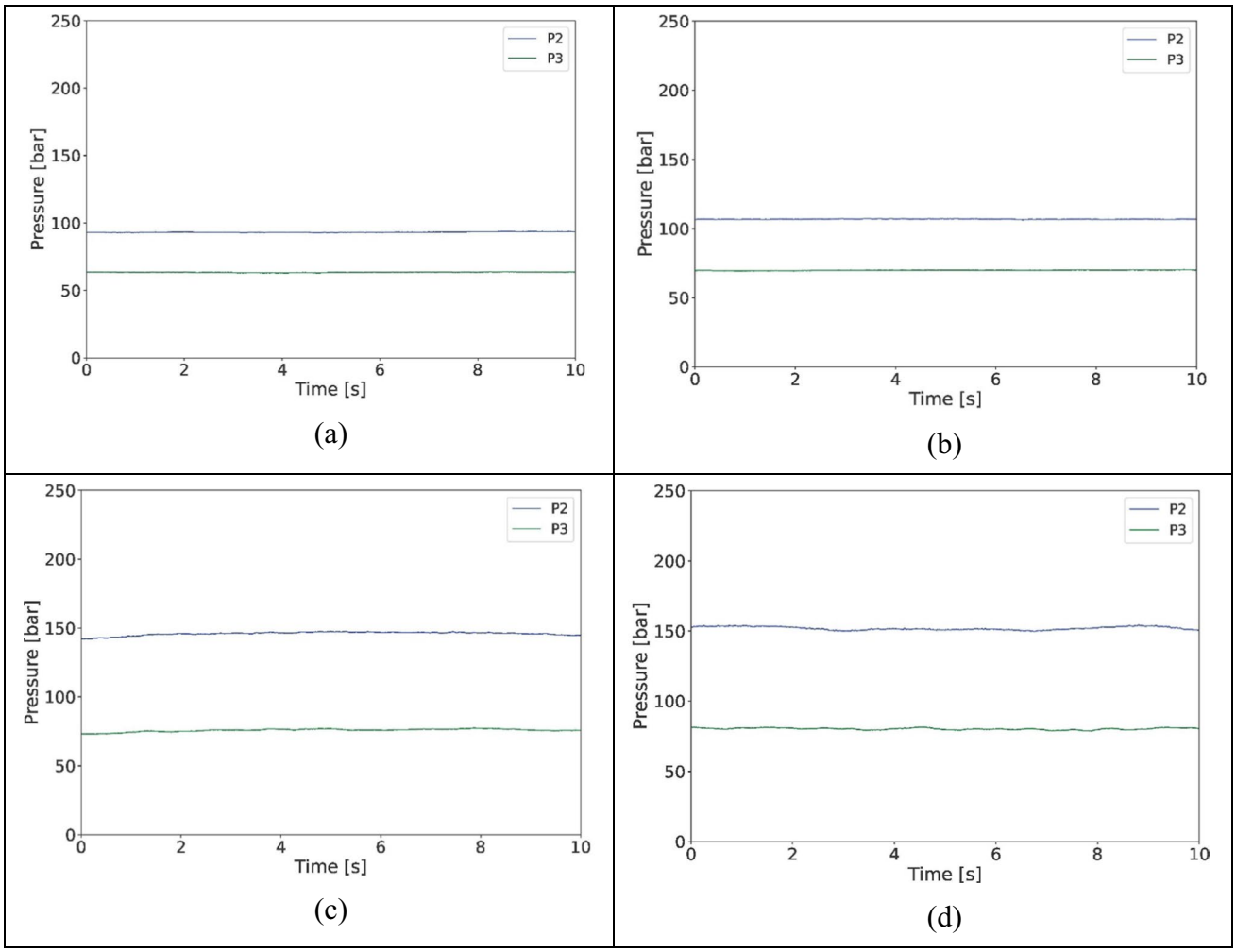

Fig. 12 Pressure data recorded with the sharkskin option for the SBR + 70 phr silica compound at shear rates **a** $\dot{\gamma}_{app} = 10\ s^{-1}$, **b** $\dot{\gamma}_{app} = 33\ s^{-1}$, **c** $\dot{\gamma}_{app} = 60\ s^{-1}$, and **d** $\dot{\gamma}_{app} = 200\ s.^{-1}$

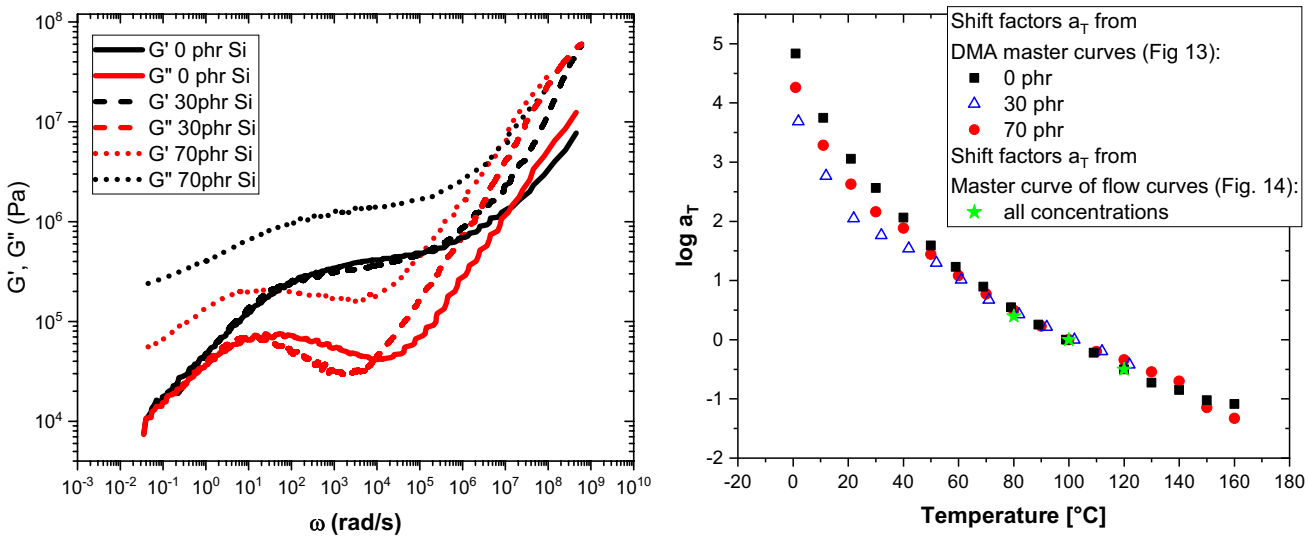

Fig. 13 Left: master curves for the elastic moduli G′ and G″ of three compounds. Right: corresponding horizontal shift factors a_T and shift factors a_T from flow curves, see text

Table 2 Parameters of the VFT fits of the a_T curves

Compound	T_{VFT} (K)	E/R (K)
0	176	2147
30	221	712
70	154	2532

Fig. 13 shows the master curves for the shear moduli G′ and G″ of the three compounds. The right side shows the corresponding horizontal shift factors a_T. Table 1 contains the values of the shift factors at the three distinct temperatures 80 °C, 100 °C (reference temperature), and 120 °C. These values have been determined from Vogel Fulcher Tamman (VFT) fits to the a_T data:

$$\log a_T = \frac{E}{R}\left(\frac{1}{T - T_{VFT}} - \frac{1}{T_0 - T_{VFT}}\right)$$

with R universal gas constant, E activation energy, and T_{VFT} VFT temperature. Table 2 shows the VFT parameters determined from the fits. It should be stressed that an analysis of the activation energies and the VFT temperatures is not in the scope of this study. The fits are only used to obtain the values of the shift factors given in Table 1.

From Fig. 13, it follows that in the temperature range between 80 °C and 120 °C where the flow curves have been recorded, the a_T parameters are almost independent of the filler content. The temperature-frequency superposition or temperature–time-superposition (TTS) is standard procedure in rotational rheology. We will not apply a similar superposition principle for the shear rates, to create a master curve (Fig. 14) from the flow curves shown in Figs. 3, 4, and 5:

$$\dot{\gamma}_p(T_0) = \dot{\gamma}_p(T) \cdot a_T$$

The obtained shift factors a_T are shown in Fig. 13 right (stars) and Table 1. Figure 13 right suggests that the shift factors obtained from the flow curves and the ones obtained from the DMA measurements show the same temperature dependency, independent of the filler content for the compounds 0 phr, 30 phr, and 70 phr and for the (relatively small) temperature range between 80 °C and 120 °C.

Conclusions

The flow curves show that for a given temperature, a longer capillary leads to a more pronounced separation of the branch I, the plateau region, and branch II. This effect diminishes with increasing temperature. This is reasonable if the plateau is linked to the onset of slip, as at a lower temperature, rubber compounds will slip easier, leading to a more pronounced plateau region. By pronounced, we mean the change in slope from the branch I to the plateau is greater.

The change of slope of the flow curve is largely independent of the filler content. One hundred twelve phr corresponds to 38 wt% (weight percent), but mainly the properties of the polymer define the onset of the plateau, as all the samples lead to a plateau starting at a similar shear rate as the unfilled SBR. Only higher-filled compounds above 30 phr show a second branch after the plateau in accordance with Crié et al. (2015).

The onset of the plateau is strongly temperature dependent and with increasing temperatures, it is shifted to higher

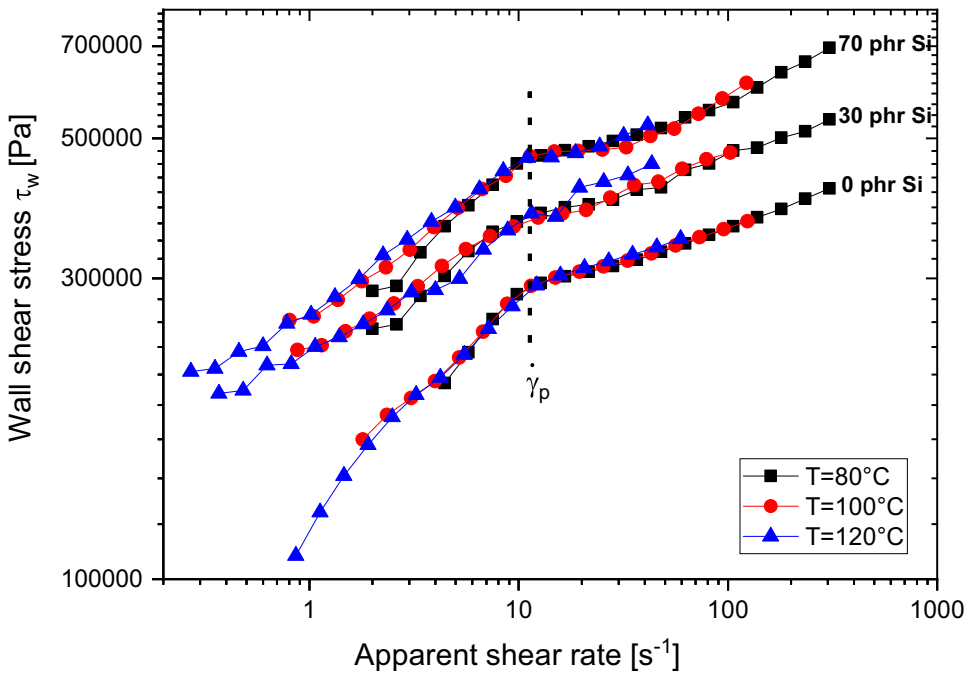

Fig. 14 Master flow curves for the different compounds

shear rates. Is there a link between the sharkskin instability and the change of slope in the flow curve (transition branch I-plateau) or is slip the dominant factor? Using the sharkskin option and measuring at specific shear rates inside branch I, plateau, and branch II, a melt instability could only be detected for unfilled SBR. However, as mentioned above, all the compounds show the changes in the flow curve, leading us to the conclusion that slip, not sharkskin as in PE (Palza et al. 2010a, b), is responsible for the onset of the plateau region in SBR.

Furthermore, it could be shown that the shear rate at which a change of slope occurs in the flow curves shows the same temperature dependency as the viscoelastic properties of the compounds. In the temperature and silica concentration range studied, it is almost independent of the filler content.

Funding This work was funded by the Luxembourg National Research Fund (FNR) and by Goodyear Innovation Center Luxembourg with grant C-PPP17/MS/11617214/SLIPEX in FNR's CORE-PPP program.

Data availability Available on request.

Code availability Not applicable.

Declarations

Conflict of interest The authors declare no competing interests.

References

Agassant J-F, Arda D, Combeau C, Merten A, Muenstedt H, Mackley M, . . . Vergnes B (2006). Polymer processing extrusion instabilities and methods for their elimination or minimisation. Int Polym Process, 21(3), pp. 239-255. https://doi.org/10.3139/217.0084

Crié A, Baritaud C, Valette R, Vergnes B (2015) Rheological behavior of uncured styrene-butadiene rubber at low temperatures, pure and filled with carbon black. Polym Eng Sci 55(9):2156–2162. https://doi.org/10.1002/pen.24090

Denn MM (2001) Extrusion instabilities and wall slip. Annu Rev Fluid Mech 33(1):265–287. https://doi.org/10.1146/annurev.fluid.33.1.265

Filipe S, Vittorias I, Wilhelm M (2008) Experimental correlation between mechanical non-linearity in LAOS flow and capillary flow instabilities for linear and branched commercial polyethylenes. Macromol Mater Eng 293(1):57–65. https://doi.org/10.1002/mame.200700194

Gansen A, Řehoř M, Sill C, Polińska P, Dheur J, Hale J, Baller J (2020) Investigation of the sharkskin melt instability using optical Fourier analysis. J Appl Polym Sci 137(24):48806. https://doi.org/10.1002/app.48806

Georgantopolus C, Esfahani M, Botha C, Naue I, Digenouts N, Causa A, . . . Wilhelm M (2021). Mechano-optical characterization of extrusion flow instabilities in styrene-butadiene rubbers: investigating the influence of molecular properties and die geometry. *Macromolecular Materials and Engineering*, 2000801–2000819. https://doi.org/10.1002/mame.202000801

Hill D, Hasegawa T, Denn M (1990) On the apparent relation between adhesive failure and melt fracture. J Rheol 34(6):891–918. https://doi.org/10.1122/1.550105

Merten A, Schwetz M, Muenstedt M (2002) Simultaneous measurements of pressure and velocity oscillations during spurt flow of a high-density polyethylene. *Proceedings of the 6th European Conference on Rheology*, pp. 147–148

Mongruel A, Cartault M (2006) Nonlinear rheology of styrene-butadiene rubber filled with carbon-black or silica particles. J Rheol 50(2):115–135. https://doi.org/10.1122/1.2167448

Myrubbercouncil. (2021, 02 15). Retrieved from http://www.myrubbercouncil.com/industry/world_production.php

Naue I (2013) Development of improved rheometric tools and their application on the non-Newtonian rheology of polymeric fluids. PhD thesis, KIT Karlsruhe. https://publikationen.bibliothek.kit.edu/1000041170.

Naue I, Kadar R, Wilhelm M (2015) A new high sensitivity system to detect instabilities during the extrusion of polymer melts. Macromol Mater Eng 300(11):1141–1152. https://doi.org/10.1002/mame.201500148

Palza H, Naue I, Wilhelm M (2009) In situ pressure fluctuations of polymer melt flow instabilities: experimental evidence about their origin and dynamics. Macromol Rapid Commun 30(21):1799–1804. https://doi.org/10.1002/marc.200900296

Palza H, Filipe S, Naue I, Wilhelm M (2010a) Correlation between polyethylene topology and melt flow instabilities by determining in-situ pressure fluctuations and applying advanced data analysis. Polymer 51(2):522–534. https://doi.org/10.1016/j.polymer.2009.11.050

Palza H, Naue F, Filipe S, Becker A, Sunder J, Göttfert A, Wilhelm M (2010b) On-line detection of polymer melt flow instabilities in a capillary rheometer. KGK 63(10):456–461

Theconversation. (2021, 02 25). Retrieved from http://theconversation.com/the-world-of-plastics-in-numbers-100291

Vergnes B (2015) Extrusion defects and flow instabilities of molten polymers. Int Polym Process 30(1):3–28. https://doi.org/10.3139/217.3011

Viloria M, Valtier M, Vergnes B (2017) Volume instabilities in capillary flow of pure SBR and SBR compounds. J Rheol 61(5):1085–1097. https://doi.org/10.1122/1.4999061

Wang S-Q (1999). Molecular transitions and dynamics at polymer, wall interfaces: origins of flow instabilities and wall slip. In *Polymers in Confined Environments* 227–275. https://doi.org/10.1007/3-540-69711-x_6